Aerosp. Sci. Technol. 5 (2001) 135–146

S1270-9638(00)01089-0/FLA

Thermo-mechanical design aspects for primary composite structures of large transport aircraft *

Dieter Petersen [1], Raimund Rolfes, Rolf Zimmermann

DLR Institute of Structural Mechanics, Lilienthalplatz 7, 38108 Braunschweig, Germany

Received 20 July 1999; revised and accepted 20 November 2000

Abstract

Thermo-mechanical design aspects for primary carbon fibre reinforced plastics (CFRP) components, especially wings, of future large transport aircraft are discussed. Numerical simulations of the heating of a wing under intensive sun irradiation and of cooling during taxiing and take-off result in the recommendation of an appropriate design temperature. The study of flat stringer-stiffened panels reveals the influence of imperfections and boundary conditions on the buckling load under simultaneous thermal and mechanical loading. © 2001 Éditions scientifiques et médicales Elsevier SAS

thermo-mechanics / heat transfer / thermal analysis / thermally induced buckling / structural stability / composites / transport aircraft / wing / fuselage

Zusammenfassung

Thermomechanische Entwurfsaspekte für Faserverbund-Primärstrukturen großer Transportflugzeuge. Thermomechanische Entwurfsaspekte für CFK-Primärkomponenten zukünftiger großer Transportflugzeuge, insbesondere für Flügel, werden diskutiert. Numerische Simulationen der Erwärmung eines Flügels unter intensiver Sonneneinstrahlung und der Abkühlung während des Rollens und des Startens resultieren in einer Empfehlung für eine geeignete Entwurfstemperatur. Die Untersuchung ebener, stringer-versteifter Paneele zeigt den Einfluß der Imperfektionen und der Randbedingungen auf die Beullast auch unter gleichzeitiger thermischer wie mechanischer Last. © 2001 Éditions scientifiques et médicales Elsevier SAS

Thermomechanik / Wärmeübertragung / Thermalanalyse / Thermisch induziertes Beulen / Strukturstabilität / Verbundwerkstoffe / Transportflugzeuge / Flügel / Rumpf

1. Introduction

For a long time composite structures have been used for secondary structures of Large Transport Aircraft (LTA). The application of composite technology for primary structures proceeded very reluctantly. Confidence in these materials was not sufficient, due to limited experience. However, the increasing pressure of international competition has recently strongly stimulated considerations of applying composites to primary structures. The new Airbus A340-500/600 will have a composite pressure bulkhead and keel beam. Nevertheless, the application of composites to wing and fuselage shells is still pending. In this context problems still have to be

* This article was presented at ODAS 1999.

[1] Correspondence and reprints.
E-mail address: Dieter.Petersen@dlr.de (D. Petersen).

solved, such as efficient fabrication methods and procedures, simulation of damage and damage tolerant design, as well as thermo-mechanical behaviour of composite wing and fuselage.

The present paper focuses on the design aspects of primary structures for LTA with carbon fibre reinforced plastics (CFRP) under combined thermal and mechanical loading. The obvious reasons for investigation are the temperature-dependent property of the matrix, the different thermal expansion ratios of plies in a multidirectional laminate due to the variation of fibre orientation, and the amount of accumulated thermal expansion with large dimensions of a structural component.

During a mission cycle the thermal input to an aircraft structure ranges from ambient temperature on ground to a very low temperature during flight, e.g. about $-50°C$ at 30 000 ft height. On the ground an additional temperature increase is obtained during stays in tropical and arid places. A temperature level beyond the glass transition point of the matrix material must be avoided, because the structural behaviour will change from an elastic to a thermo-viscoelastic or a thermo-plastic one with loss of stiffness and strength. On the other hand side, the low temperatures will cause brittleness. Additionally, repeated temperature changes will intensify ageing.

The first part of this paper commences with the prerequisites necessary for the investigation of thermo-mechanical behaviour, i.e. the analysis of the temperature distribution in a structural component, which in turn is based on the knowledge of thermo-physical properties. The outer wing of the future airliner A3XX is taken as an illustrative example for a primary composite structure. The effects of different structural concepts and surface properties aimed at limiting temperature levels are outlined. Thus, the paper does not either deal with loss of strength and stiffness of composites heated to a high degree nor with ageing under thermal cycling. However, the second part is primarily devoted to the structural stability of composite panels under combined thermo-mechanical loading.

2. Steady state and transient temperature distributions in a CFRP wing box

The analysis of the transient temperature distribution of composite primary structures is needed for determining a design temperature. This is required for two reasons. Firstly, it serves for the determination of material properties, which depend on temperature, and secondly, temperature constitutes an additional load case, the influence of which must be superimposed to the mechanical loads.

More specifically, the subsequent thermal analysis of the outer wing of the future MegalinerA3XX aims at answering the following questions:

(1) what is the maximum temperature of the composite wing when exposed to sun irradiation at a high altitude airport?
(2) what time is needed for heating the wing from a uniform temperature equal to ambient air temperature?
(3) what is the cooling behaviour of the wing during taxiing and take-off?

Furthermore, parameters shall be taken into account which either depend on the wishes of the customers (e.g. colour of the wing paint) or are subject to design changes (e.g. skin thickness).

Papers on design temperatures for thermally loaded composite structures are very rare in the published literature. Stauffer and James [14] have investigated a composite vertical fin subjected to sun irradiation at an angle of 45° and came up with a design temperature of 355 K, which occurred after taxiing. They assumed that design loads can occur any time during take-off. Therefore, they did not take into account cooling during take-off and climb. The results cannot be applied to the wing under sun irradiation at 90°; moreover, the boundary conditions and thermo-physical properties used in [14] are not clear. New numerical tools for thermal analysis of composite structures have been suggested by several authors. A linear Thermal Lamination Theory and a related finite element were formulated by Rolfes [8]. The 2D element allows for full 3D thermal analysis and is therefore very well suited for the wing box under consideration. An iterative predictor-corrector procedure for composite plates and shells was developed by Noor and Burton [5]. For axisymmetric problems hierarchical finite elements were introduced by Surana and Orth [16]. All methods aim at avoiding a full 3D thermal analysis. Also, finite elements based on the linear or quadratic Thermal Lamination Theory could be easily implemented into existing FE packages. Since this has not been fully accomplished yet, 3D analyses using MSC/NASTRAN were carried out within the present study.

2.1. Geometry, loading and boundary conditions

A wire frame model of the outer composite wing box is depicted in *figure 1*. It consists of six sections separated by seven ribs (R32 to R38). Rib 32 constitutes the interface to the inner metallic wing box. Thermal loading due to sun irradiation is assumed constant in span and depth direction of the wing. Thus, heat transfer occurs predominantly in the thickness direction. The interface area around rib 32 is influenced by the adjacent metallic wing box and is therefore excluded from the subsequent investigations. Two half sections (models R33 and R38) representing areas of low and high wall thickness were selected for the finite element analyses. *Figure 2* shows the discretisation of model R33 using 8-noded HEXA elements. Convergence studies were conducted in order to reveal the minimum number of elements required

in the thickness direction of the laminates. Using two elements resulted in a maximum error of 2.2% of the total temperature difference as compared to five elements. Moreover, the maximum errors occurred in transient analyses during the first few time steps. Towards steady state the errors declined rapidly. Thus, two elements were selected for discretisation in thickness direction. The conductivity tensor of a HEXA element was calculated by averaging the tensors of all layers within the element. Thus, the sequence of stacking was neglected, which is acceptable for dominating transverse heat transfer but not applicable in case of full 3D heat transfer. The latter case requires layerwise discretisations or Thermal Lamination Theories e.g. [11]. Geometry and stacking sequence of the structural parts are summarised in *table I*.

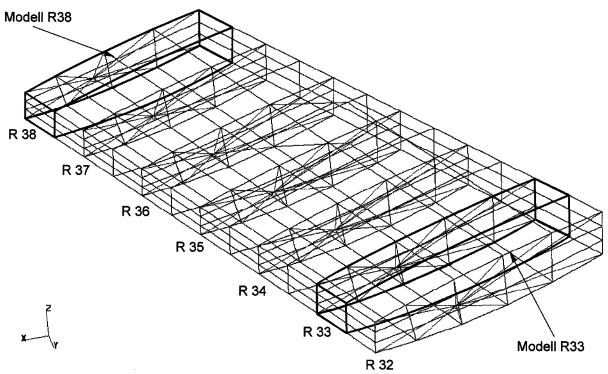

Figure 1. Wire frame model of composite wing box.

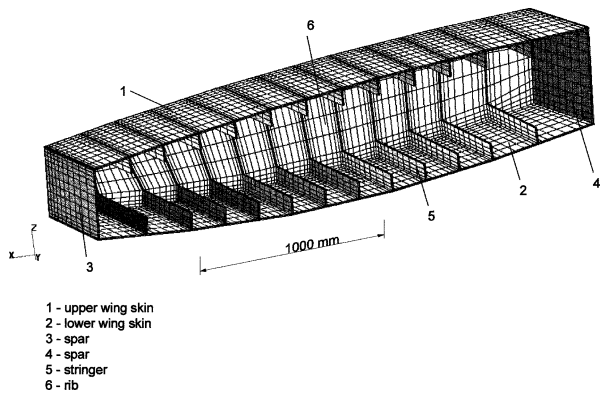

Figure 2. Finite element model R33.

The wing box is heated up by sun irradiation, the solar heat flux increases significantly with altitude. On a high altitude airport at 3500 m above sea level there is a solar heat flux of

$$q_s = 1082 \frac{W}{m^2}. \tag{1}$$

This leads to an absorbed heat flux of

$$q_{at} = \alpha_w q_s \tag{2}$$

on the upper wing surface, where α_w denotes the solar absorptivity of the wing. The lower surface is heated by radiation reflected from the ground,

$$q_{ab} = \alpha_w (1 - \alpha_g) q_s, \tag{3}$$

where α_g is the absorptivity of the ground. Both surfaces also radiate heat against the environment according to the Stefan–Boltzmann law

$$q_e = \varepsilon_w \sigma_{SB} \left(T_{surf}^4 - T_\infty^4 \right). \tag{4}$$

ε_w is the thermal emissivity of the wing, σ_{SB} the Stefan–Boltzmann constant and T_{surf} the surface temperature. The temperature of the radiation background T_∞ is, for the upper skin, equal to the ambient temperature T_{amb} and for the lower skin equal to the ground temperature. There is also internal radiation exchange between skins, stringers, ribs and spars which might be taken into account. However, calculating the radiation exchange matrix is very costly and introducing the matrix into the heat transfer analysis destroys the banded structures of the equation system. An example calculation has shown that the temperature of the upper skin is decreased by not more than 6% of the total temperature difference when taking into account internal radiation exchange. Neglecting the effect in the subsequent parametric studies safes

Table I. Geometry and stacking sequence of structural parts of CFRP wing.

Structural part	Lay-up [°]	Percentage of layers $0°/\pm 45°/90°$ [%]	Model R33 thickness [mm]	Model R38 thickness [mm]
Skins(1/2)	$(+0_2 - 90 + 0_2 - 0)_{s2}$	50/40/10	9.50/8.00	5.00/4.50
Spars(3/4)	$(+ - + - 90 + -0 + -)_{s2}$	10/80/10	8.70/9.60	7.00/7.75
Rib(6)	$[(+90_2 - 0_2 + 90_2 -)_2]_s$	20/40/40		
Stringers(5)	$(+0_3 - 90 + 0_3 - 0_3 90 - 0_3 +)_s$	60/30/10	8.50 ($h = 76.9$)	7.75 ($h = 61.8$)
		$+ = +45°; - = -45°$		
		$()_{sn}$ = symmetry; n – times		

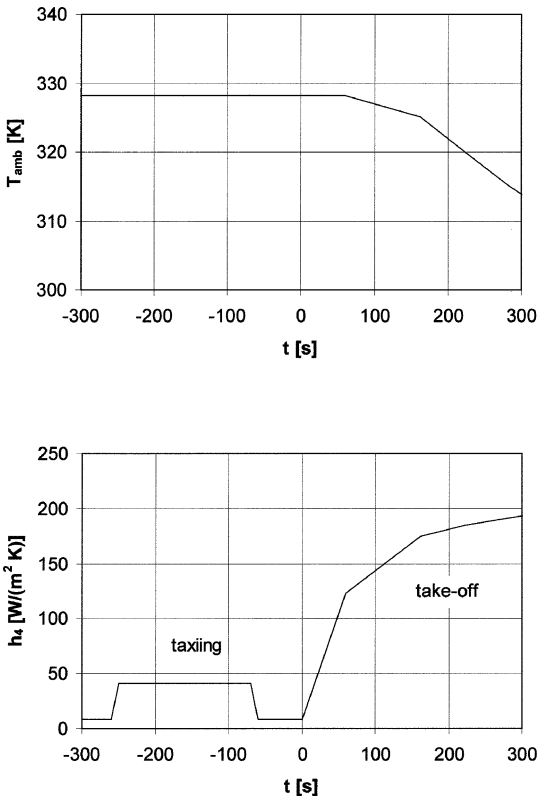

Figure 3. Ambient temperature and convection coefficient versus time for taxiing and take-off.

a huge amount of computing time and provides temperatures on the safe side. Another important boundary condition is convection, which can be described by the Newtonian law

$$q_c = h(T_{surf} - T_{amb}), \tag{5}$$

where q_c is the convective heat flux and h the convection coefficient. Free convection applies when the aircraft is standing on the ground, forced convection occurs during taxiing and take-off. For fluid flow about a surface the convection coefficient can be calculated from the Nußelt number Nu, the length of the surface l and the thermal conductivity λ_{fl} of the fluid according to

$$h = \frac{Nu\lambda_{fl}}{l}. \tag{6}$$

The Nußelt number in turn can be determined from the Reynolds and the Prandtl numbers where different equations apply for laminar and turbulent flow e.g. [1]. Applying this procedure resulted in the coefficient for forced convection as depicted in *figure 3*. It mainly depends on the velocity of the aircraft. However, it should be mentioned that the convection coefficient based on the Nußelt number is only an approximation. For achieving accurate values a measurement is necessary which uses the original surface roughness of the aircraft paint. Such results can be found in [13]. The decreasing ambient temperature during climb is also shown in *figure 3* and must be taken into account when evaluating equation (5). Convection can also take part in the interior of the wing box if it is not fully insulated. An open system (*figure 4*) can exchange heat with the environment. For very high exchange rates the interior air temperature can become equal to the ambient temperature. In the present case the exchange rate can be low in some cases since there will be wing sections without any opening. In case of a fully insulated closed system (*figure 4*) with a warm wall above a cold one, convection will no longer occur. Although the wing box will always have some heat exchange through the spars the closed system must be regarded as a limiting case. The boundary planes parallel to the ribs of models R33 and R38 are assumed adiabatic due to (approximate) symmetry conditions.

The thermo-physical properties of CIBA 6376/T400 were extracted from [9] and [10] for a fibre volume fraction of 60% and an average temperature of 348 K. The epoxy resin CIBA 6376 has a glass transition temperature of 453 K under dry and of 423 K under wet conditions.

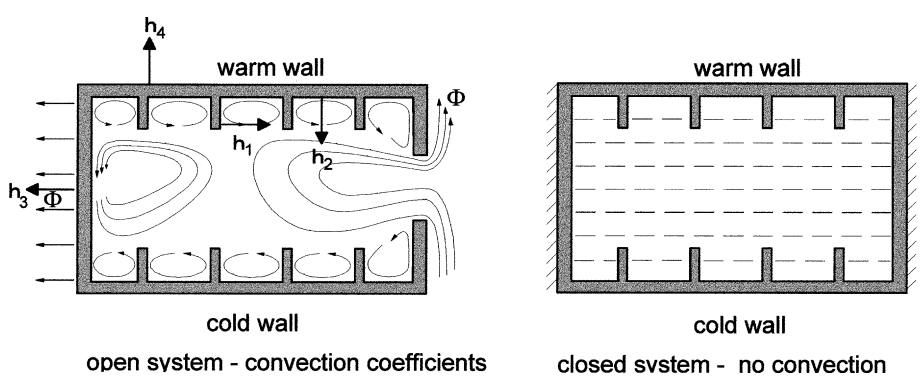

Figure 4. Comparison of convection in closed and open systems.

Table II. Thermo-physical properties and thermal boundary conditions for CFRP wing.

	Symbol	Value	
		Open system	Closed system
Solar heat flux	q_S	1082 W/m^2	1082 W/m^2
Solar absorptivity			
Wing skin	α_w	0.0, . . . , 1.0	0.0, . . . , 1.0
Airport ground	α_g	0.73	0.73
Thermal emissivity			
Wing skin	ε_w	0.0, . . . , 1.0	0.0, . . . , 1.0
Convection coefficients			
Stringers	h_1	14.5 W/m^2 K	0
Ribs, outside	h_3	7.0 W/m^2 K	0
Skin, inside	h_2	22.5 W/m^2 K	0
Skin, outside	h_4	8.5 W/m^2 K	8.5 W/m^2 K
Temperatures	T		
Outside	$T_{amb.}$	328.15 K	328.15 K
Inside	$T_{amb.}$	328.15 K	
Ground	T_g	348.15 K	348.15 K
Conductivities			
CIBA 6376/T400, parallel	λ_1	5.333 W/m K	
CIBA 6376/T400, transverse	λ_2	0.642 W/m K	
Heat capacity			
CIBA 6376/T400	c	1.059 J/gK	

Table III. Thermo-optical properties of usual surfaces.

Material	Absorptivity α_S	Emissivity ε_{th}
Gold	0.29	0.018, . . . , 0.035
Aluminium	0.10, . . . , 0.20	0.04, . . . , 0.20
Paint, white	0.20	0.90
Oil paint, white	0.30	0.90, . . . , 0.96
Oil paint, light green	0.50	0.90, . . . , 0.96
Oil paint, light grey	0.75	0.90, . . . , 0.96
Oil paint, dark blue or black	0.80, . . . , 0.90	0.90, . . . , 0.96

2.2. Steady state analyses

Steady state analyses were conducted in order to answer question (1).

Thermal loadings and boundary conditions from *table II* were used. *Table III* shows solar absorptivities and thermal emissivities of usual surfaces. All aircraft paints have emissivities of about 0.9 and differ only in the absorptivity ranging from 0.2 for white colour to 0.9 for black colour. Open and closed systems must both be considered, since they differ in the temperature distribution and in the maximum values. The closed system shows a uniform temperature field throughout upper skin and stringers due to lack of temperature exchange of the interior with the environment. However, the open system has maximum temperatures on the skin at the center between adjacent stringers. Therefore, this point is selected for studying the influence on the temperature level of various parameters. *Figures 5* and *6* show the maximum tempera-

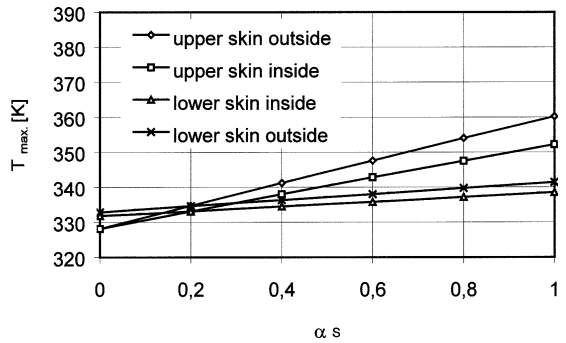

Figure 5. Maximum temperature versus absorptivity in an open system ($\varepsilon_{th} = 0.9$, model R33).

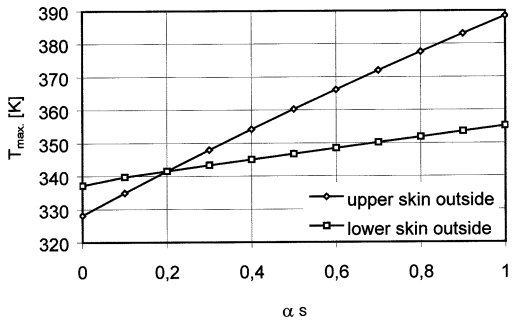

Figure 6. Maximum temperature versus absorptivity in a closed system ($\varepsilon_{th} = 0.9$, model R33).

tures of model R33 as function of the solar absorptivity for open and closed systems, respectively. The closed system generally leads to higher temperatures and reveals no difference between inner and outer surfaces of the wing skins. The influence of the absorptivity is significant in both cases. The maximum temperature achieved in the closed system with black paint is about 383 K compared to 341 K for white colour (*figure 6*). Model R38 has a lower skin thickness as compared to model R33. This has no effect on the maximum temperature when assuming a closed system, whereas a slight decrease is observed in the open system. Again, the reason is the full insulation of the interior wing box from the environment in the closed system [2]. That is why the maximum temperature depends on the absorped heat flux and the external boundary conditions only. Geometrical parameters such as skin thickness or stringers height have influence on the open but not on the closed system. The external convection coefficient, however, effects both systems. *Figure 7* shows that the maximum temperature of the closed system decreases by about 15 K when the coefficient is raised from 8.5 to 17 W/m^2 K. Somewhat smaller values were achieved for the open system. This parameter mainly depends on the velocity of the wind. Thus, the free convection coefficient of 8.5 W/m^2 K for still air should be assumed to be on the safe side. It can be summarised that even under worst case conditions (closed system,

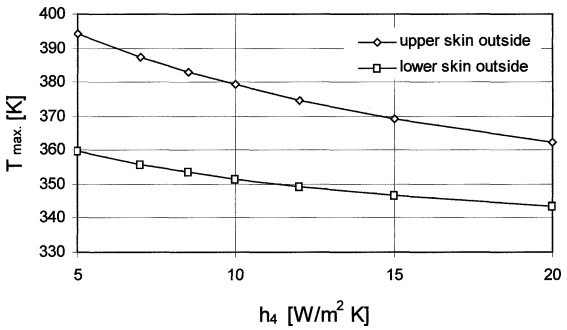

Figure 7. Maximum temperature versus free convection coefficient (black wing, model R33, closed system).

skin thickness of model R33, low convection coefficient) the temperature does not exceed 341 K and 383 K for white and black paint, respectively. This level is at least 40 K below the glass transition temperature under wet conditions.

2.3. Transient analyses

Transient analyses of the heating and cooling phase were conducted to answer questions (2) and (3).

For the heating phase a start temperature equal to the ambient temperature of 328 K was assumed which is a temperature in a tropical environment. All boundary and loading conditions as summarised in *table II* remained unchanged. The heating time was defined as the time needed for reaching a heating rate below 10^{-3} K/sec at all finite element nodes. In contrast to the steady state analyses not only maximum values but the whole temperature field was examined. For that purpose, pure skin and skin-stringer areas were regarded. *Table IV* gives the heating times for various configurations. The heating time strongly depends on the temperature level achieved at steady state. Thus, the time is higher for closed as compared to open systems and for black as compared to white paint. The difference between models R33 and R38 which was small or even negligible in the steady state case, is now very pronounced since the mass to be heated is different.

The difference between skin and skin-stringer areas in the closed system is very high. The steady state analysis has shown that in this case the stringer is uniformly heated. This process takes a long time, because the heat flow has to pass through the stringer height by conduction. This way is much longer than in case of a thin-walled panel skin. The effect does not occur in open systems, because a steady state temperature gradient in the thickness direction is preserved. The steady state analysis has shown that the maximum temperature of 383 K occurs in the closed system with black paint for both models. Under this worst case condition the smallest heating time applies to model R38 and is 2115 seconds.

Table IV. Time for heating up the CFRP wing.

	Model	$t_{\text{stationary}}$ [s]	
		Section of skin	Section of stringer
Open system	R 33; white	1095	1055
	R 33; black	1655	1655
	R 38; white	705	735
	R 38; black	995	1245
Closed system	R 33; white	2615	> 5600
	R 33; black	3595	> 5600
	R 38; white	1685	> 4600
	R 38; black	2115	> 4600

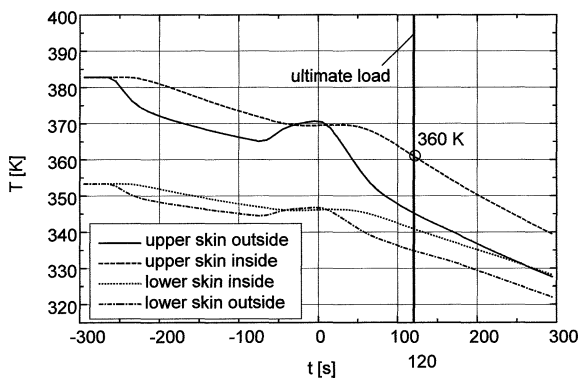

Figure 8. Cooling curve of model R33 (black wing, closed system).

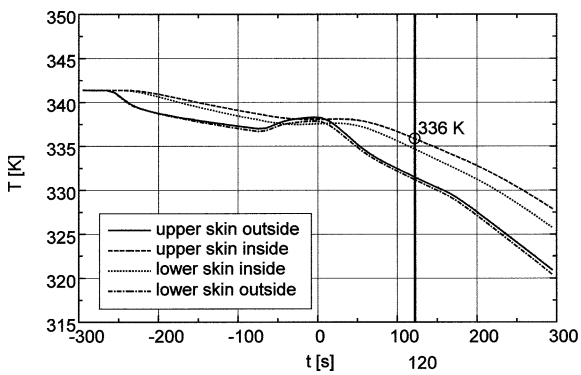

Figure 9. Cooling curve of model R33 (white wing, closed system).

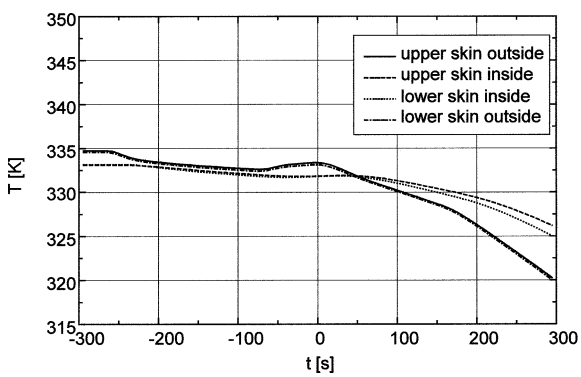

Figure 10. Cooling curve of model R33 (white wing, open system).

Using white paint shortens the time to 1685 seconds but provides a much lower temperature of about 341 K.

For simulating the cooling phase during taxiing and take-off the coefficient for forced convection from *figure 3* was applied instead of the free convection coefficient of 8.5 W/m^2 K. The steady state temperature field at the end of the heating phase was taken as initial condition. All other boundary and loading conditions did not change. *Figure 8* shows the cooling curves for model R33 with black paint (closed system). It can be observed that the outer surfaces of upper and lower wing skins cool down much faster than the inner surfaces. *Figure 9* reveals that white paint leads to a reduced cooling rate since the temperature difference between structure and fluid is lower. However, all temperature curves in *figure 9* are below the ones in *figure 8* over the whole time range. At $t = +300$ s nearly the same temperature level is reached for both colours. Switching to the open system (*figure 10*) leads to further reduction of the steady state temperature at $t = -300$ s and of the whole cooling curve. Again at $t = +300$ s the same temperature level is reached as before. In contrast to the closed system the inner surfaces of both skins become warmer than the outer surfaces only at the start. This occurred already in the closed system during taxiing since there is no internal cooling by convection. Reduction of the wall thickness leads to slightly lower temperatures of the outer surfaces and significantly lower temperatures of the inner surfaces (*figures 11* and *9*).

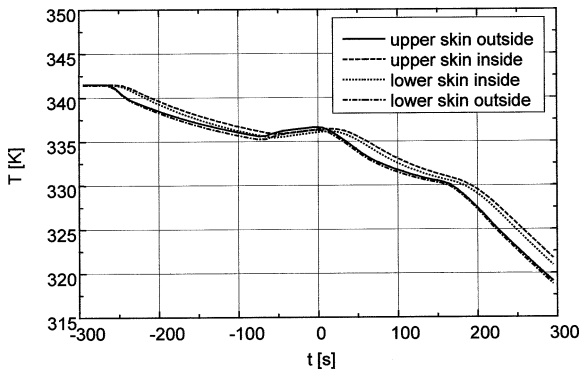

Figure 11. Cooling curve of model R38 (white wing, closed system).

As in the steady state analysis worst case conditions are again the closed system with high wall thickness (model R33). Thus, *figures 8* and *9* should be evaluated for black and white paint, respectively, when a design temperature at a distinct time is looked for.

Assuming worst case conditions as described above and a scenario where an aircraft rolls out from shadow, is loaded with passengers or freight, taxis, starts (*figure 3*) and has to sustain ultimate load not before $t = +120$ s the following can be stated. When exposed to sun irradiation the time to reach the maximum temperature of 341 K or 383 K is 1685 or 2115 seconds depending on the colour. In most cases this time will be reached during loading of the aircraft. Therefore it is realistic to start the cooling simulation with the heated up aircraft. Two minutes after beginning of start the maximum temperature of the white or black wing occurs at the inner surface of the upper skin and has decreased to 336 K or 360 K, respectively. These values can be looked upon as design temperatures.

3. Stability of CFRP panels subjected to thermo-mechanical loading

Because thin-walled light weight structures for LTA are susceptible to buckling, structural stability is the design driver for large areas of today's aircraft structures. Also, the influence of thermal loads on the buckling behaviour has been investigated by many authors (e.g. [3, 4,6,7,12,15]). However, design guidelines for combined thermo-mechanical loading are very rare.

Primary structures of different curvatures have to be considered. Many parts of the fuselage are curved, whereas the wing panels are only slightly curved or nearly flat. A thermo-mechanical design guideline for stiffened curved panels has already been established by Rolfes et al. [12]. In that study the expansion of the panel transverse to the loading direction was not restricted. The influence of an additional thermal loading on the mechanical buckling load turned out to be very low. The influence of other parameters such as temperature gradient in thickness direction or stacking sequence was negligible in that case. Such panels can be designed for pure mechanical loading.

The present study examines flat panels, which are representative in the case of LTA wing panels and especially of a supersonic transport aircraft wing. The panels exhibit such large radii that their behaviour does not differ from flat ones. This was stated by comparing computations of slightly curved panels with radii of $r = 50\,000$ mm and $r = 100\,000$ mm with a flat panel. Linear bifurcation calculations revealed the same buckling loads.

A flat stringer stiffened panel with dimensions, stacking sequence, and material properties according to [12] was investigated. The boundary conditions were modelled with respect to intended experiments as given in *figure 12(a)*. This figure also shows the finite element net. According to the THERMEX-B test facility, wrinkling of the unloaded edges was prevented by clamping with buckling supports. Also, free transverse expansion due to thermal load and Poisson's ratio was allowed in the first series of analyses to model the test site conditions. Within an additional series of calculations the transverse expansion of the panel was restrained.

Special care was devoted to modelling realistically the junction area between stringer flanges and skin [12]. The panel itself was designed for global buckling which is indicated by the first and second buckling mode (*figure 12(b)* and *(c)*). Geometrical imperfections were modelled in the form of these modes with amplitudes of 0.1 and 0.3 mm (6.7 and 20% of the skin thickness).

Non-linear computations using the finite element code ANSYS were carried out for the geometrically ideal panel and panels with the two different imperfection amplitudes of the second mode shape. The buckling point was defined as the load, which could be achieved just before the algorithm failed to converge. For all three computations a non-linear buckling load of 94.8 kN was obtained and a buckling mode shaped like the first mode occurred. The snap-through took place at a load of 87.5 kN. In case of imperfections in form of the first mode the computations again failed to converge at a load of 94.8 kN. In both cases of imperfect shapes the behaviour was identical. Global buckling of the plate was obtained, which turned out to be independent of the out-of-plane imperfection shape. Curved panels, however, are significantly influenced by out-of-plane imperfections (e.g. [12]). This can be explained by fully different post-buckling behaviour of flat and curved panels.

Moreover, in-plane imperfection, i.e. inhomogeneous load introduction was simulated to study whether this effect could be important in establishing design guidelines for realistic structures. Varying at one of the loaded edges the boundary displacement with the coordinate y was the measure to apply an in-plane imperfection. Either a linear or a sinusoidal imperfection with one or three half waves was considered. *Table V* shows that the sinusoidal im-

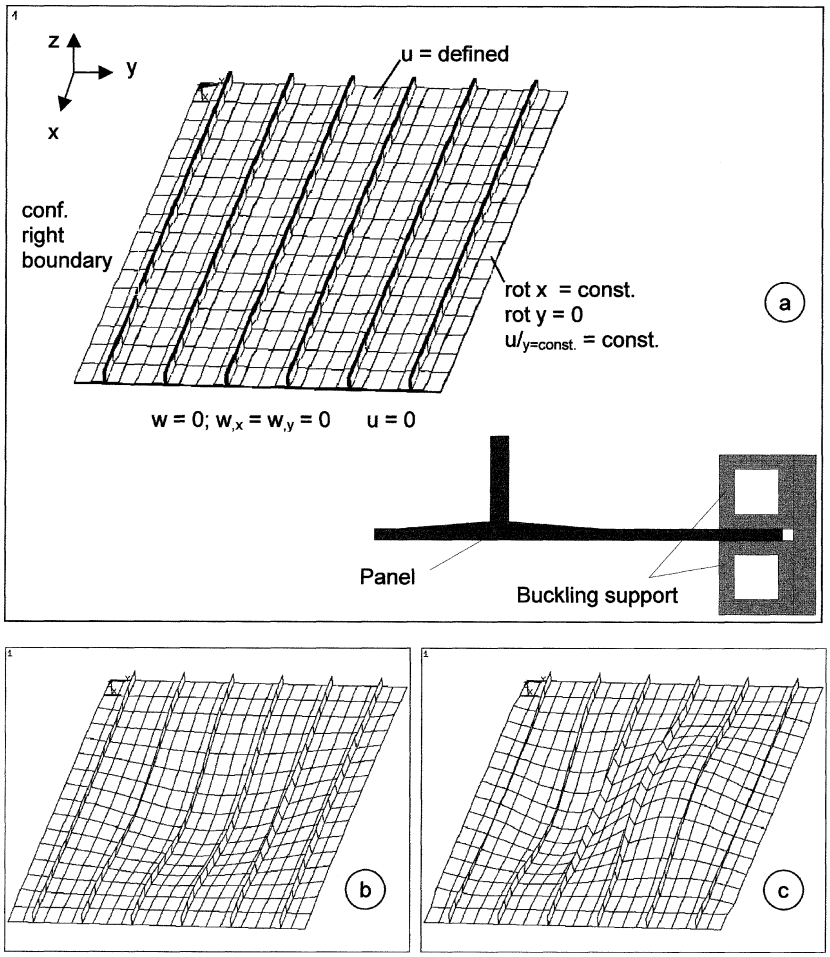

Figure 12. Flat panel with six stringers for investigation of imperfection sensitivity.

Table V. Influence of load imperfections on nonlinear buckling load of flat stringer-stiffened panel.

Form of imperfection (load introduction)	Amplitude of imperfection [mm]	Nonlinear buckling load [kN]
None	0	97.2
Sinusoidal, one half-wave	0.025	81.7
Sinusoidal, one half-wave	0.05	81.5
Sinusoidal, one half-wave	0.1	83.6
Sinusoidal, one half-wave	0.15	80.9
Linear	0.05	86.3
Sinusoidal, three half-waves	0.025	86.4
Sinusoidal, three half-waves	0.05	86.5
Sinusoidal, three half-waves	0.15	87.4

perfection with one half wave in y direction leads to the largest reduction of the non-linear buckling load, which is about 15%. Both other imperfections have a smaller influence on the buckling load, because they either create the maximum load near the unloaded boundary stiffened by the buckling support (linear imperfection) or they

show areas of unloading near to the mostly loaded central section (sinusoidal imperfection with three half waves). However, the amplitude of the imperfection has a minor influence. Already 0.025 mm (1.9% of the shortening at buckling load) suffice for significantly reducing the non-linear buckling load. The buckling load of the perfect panel is now somewhat higher than before (97.2 kN compared to 94.8 kN), because another material was used.

A principal result of these calculations has been that a flat stringer-stiffened panel designed for global buckling is insensitive to out-of-plane imperfections, but very sensitive to in-plane ones, i.e. compression load imperfections.

Temperature is an additional load case, which generates thermal strains and stresses in anisotropic CFRP panel. Even, a uniform temperature field yields out-of-plane displacements similar to the first mode (*figure 12(b)*), because the plate is stiffened only at one side. Therefore temperature loading can also be looked upon as a special case of geometrical imperfection.

A thermal model to calculate the temperature distribution was also developed to apply a thermal load. It consisted of thermal solid elements with the temperature as the only degree of freedom. Temperatures on the outer surface of the panel were directly applied to the FE nodes as a predefined temperature. On the inner side of the panel free convection was applied to the element surfaces. Thus, test conditions were numerically simulated.

The panel depicted in *figure 12* with $(+-45,0)_s$- and $(+-45,0_3)_s$- lay-ups for skin and stringer, respectively, and with temperature-dependent material properties for CIBA 6376/HTA listed in *table VI* was subjected to combined thermal and mechanical loading. This material was finally chosen for two reasons. In the first place, the temperature-dependent material data were sufficiently available. Secondly, an in-house manufacturing of panels for experimental verification could be provided. The decisive elastic modulus in compression decreased only slightly compared to the material of the previous investigations. For this reason, the buckling load remained nearly the same (93.3 kN). Also, the buckling behaviour did not change.

Table VI. Temperature dependent material properties of CIBA 6376/HTA.

Temperature	298 K	363 K
E, x	125000 N/mm^2	125000 N/mm^2
E, y	10000 N/mm^2	9000 N/mm^2
E, z	10000 N/mm^2	9000 N/mm^2
G, xy	6000 N/mm^2	5000 N/mm^2
G, xz	6000 N/mm^2	5000 N/mm^2
G, yz	3600 N/mm^2	3400 N/mm^2
Pr, xy	0.34	0.29
Pr, xz	0.34	0.29
Pr, yz	0.38	0.32
alpha, x	$1.09e-7\,K^{-1}$	$3.34e-7\,K^{-1}$
alpha, y	$3.35e-5\,K^{-1}$	$3.46e-5\,K^{-1}$
alpha, z	$3.35e-5\,K^{-1}$	$3.46e-5\,K^{-1}$

The results of a linear bifurcation analysis are given in *figure 13(a)*. They show that there is basically no reduction of the buckling load due to temperature increase within a realistic range up to 150 °C. This is underlined by geometrically and physically non-linear calculations using the arc length method which yielded identical load shortening curves for 25 °C and 100 °C (*figure 13(b)*). Degradation of the material properties was taken into account but obviously had only minor influence on the buckling load. Regarding temperature loading as a special case of geometrical imperfections this behaviour agrees with the non-sensitivity of the flat panel to out-of-plane imperfections as well as with the non-sensitivity of curved panels [12] to temperature.

In all investigations carried out so far the transverse expansion of the panel was unrestrained. Within the next step of simulation the unloaded edges were fixed

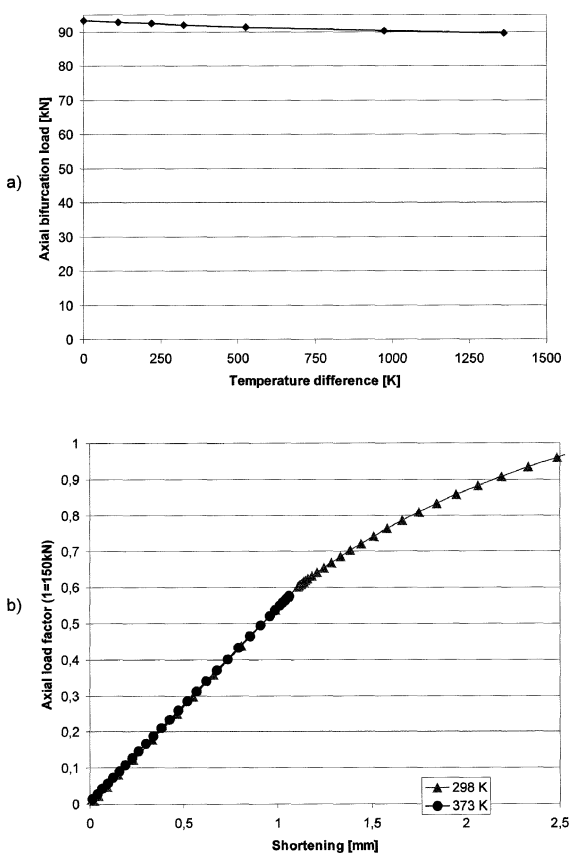

Figure 13. Influence of temperature on buckling load of flat panel with free transverse expansion; a) Axial bifurcation load versus temperature difference (linear analysis); b) Load-shortening curves (nonlinear arc-length analysis).

in transverse and normal direction ($v = w = 0$) and the rotations were left free. Thus, the influence of the transverse expansion could be studied. *Figure 14* shows that the buckling load under pure mechanical load is less than half of the value obtained before. In contrast to the free transverse expansion, a very pronounced reduction of the buckling load due to temperature increase could now be observed. At the design temperature of 336 K (43 K above room temperature) for a white painted wing which has been calculated in section 2, the buckling load is only 34% of the one at room temperature.

The panel design studied with the $(+/-45°, 0°)_s$ skin lay-up resulted in a rather large transverse expansion ratio under mechanical shortening as well as under thermal loading. Therefore, both extremes, maximum transverse expansion with only 0° plies in the skin, and minimum transverse expansion with only 90° plies in the skin, were studied (*table VII*). Linear bifurcation analyses were performed considering pure axial shortening and pure thermal loading at restrained transverse expansion. The 0°-only skin lay-up panel reached a mechanical bifurcation load of 85.3 kN, but the buckling temperature difference was only 18.5 K. The 90°-only skin lay-up panel showed a mechanical bifurcation load of 60.6 kN, but the buckling temperature difference increased up to 115.6 K. On the bases of these calculations, a skin lay-up optimisation was performed under the prescription of mechanical buckling load maximisation at room temperature under the restrained boundary conditions explained above. A maximum buckling load of 86.3 kN was reached with a $(90°, 0°)_s$ skin lay-up. The buckling temperature difference for this panel design was 88.6 K, which was considered very high.

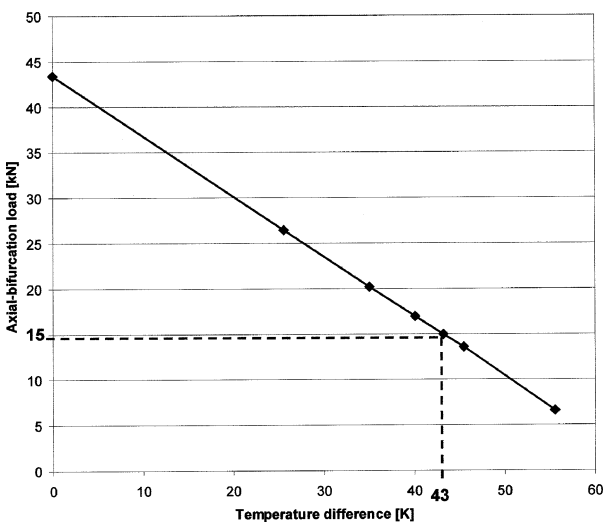

Figure 14. Influence of temperature on buckling load of flat panel with restricted transverse expansion; axial bifurcation load versus temperature difference.

In conclusion, the buckling behaviour of a flat, axially stringer-stiffened CFRP-panel depends on its boundary conditions, especially in transverse direction. Lay-up of skin designs resulting from optimisation calculations under pure mechanical loading differ significantly for the considered boundary conditions. But for both designs, it can be deduced that an optimised lay-up of the skin for a maximum buckling load under pure mechanical loading is also appropriate under additional thermal loading conditions.

The boundary conditions of a panel in a real wing box with ribs and spars will reside between the boundary conditions considered in this paper. The stiffness of the elastic restraint must be extracted from a global analysis of the wing structure.

4. Conclusions

Application of CFRP primary structures to future large transport aircraft calls for much more careful investigation of thermo-mechanical behaviour than for metallic structures. By the example of a composite wing structure thermal analyses of heating and cooling phases during standing at an airport, taxiing and take-off and analyses of thermo-mechanical buckling were performed to discuss design aspects. Other phenomena such as loss of strength and stiffness, if composites are heated beyond the glass transition temperature of the resin, and thermally induced ageing have not been considered.

Maximum temperatures under sun irradiation at the airport were calculated between 341 and 383 K depending on the colour. Cooling during taxiing and take-off leads to reduced temperatures between 336 and 360 K which act two minutes after starting. Assuming that ultimate load occurs at that earliest time, theses values can be looked upon as design temperatures. The coefficient describing the forced convection during the cooling phase was calculated from the Nußelt number. Using measured convection coefficients the analysis results should

Table VII. Mechanical bifurcation buckling loads and critical temperature differences for variations of skin lay-up.

Panel skin-layup	Mechanical bifurcation load [kN]	Critical temperature difference [K]
0°	85.3	18.5
90°	60.6	115.6
$(90°, 0°)_s$	86.3	88.6

be checked. Investigations of flat stringer-stiffened panels showed a very decisive influence of the boundary conditions on the sensitivity to thermo-mechanical buckling. Whereas under free transverse expansion nearly no reduction of the mechanical buckling load could be observed due to temperature increase, the buckling load dropped to only 34% at design temperature (341 K for white colour) when restricting the expansion. Therefore, the boundary conditions of a panel in a real wing box must be extracted from a global analysis of the wing structure. Nevertheless, using optimisation methods it could be revealed that an optimised lay-up of the skin for maximum buckling load under pure mechanical loading is also appropriate for additional thermal loading conditions.

References

[1] Elsner N., Grundlagen der technischen Thermodynamik, Band 2, Berlin, Akademie Verlag, 1993.

[2] Herold S., Rolfes R., Noack J., Thermalanalyse eines CFK-Flügels, DLR Report IB131-98/37, Braunschweig, 1998.

[3] Meyers C.A., Hyer M.W., Thermal buckling of symmetrically laminated composite plates, mechanics of composites at elevated and cryogenic temperatures, in: Proc. Symposium, ASME Applied Mechanics Conf., Columbus, OH, June 16–19, 1991; NY, ASME, 1991, pp. 287–303.

[4] Noor A.K., Thermomechanical buckling and postbuckling of multilayered composite panels, AIAA Paper 92-2541, 1992.

[5] Noor A.K., Burton W.S., Steady-state heat conduction in multilayered composite plates and shells, Comput. Struct. 39 (1991) 185–193.

[6] Noor A.K., Burton W.S., Three-dimensional solutions for the thermal buckling and sensivity derivates of temperature-sensitive multilayered angle-ply plates, J. Appl. Mech-T ASME 59 (4) (1992) 848–856.

[7] Rohwer K., A further study on thermal buckling of simply supported antimetricangle-ply laminates in a uniform-temperature field, Compos. Sci. Technol. 46 (1) (1993) 85–86.

[8] Rolfes R., Efficient thermal analysis of anisotropic composite plates using new finite elements, in: Füller J., et al. (Eds.), Developments in the Science and Technology of Composite Materials, Proc. 4th European Conf. on Composite Meterials (ECCM4), Stuttgart, 1990, Elsevier Applied Science, London 1990, pp. 743–748.

[9] Rolfes R., Wärmeleitzahlen von UD-Laminaten aus CFK, Berechnung und Messung, DLR Report IB131-91/12, Braunschweig, 1991.

[10] Rolfes R., Schmidt K., Thermalanalyse von Strukturteilen aus CFK, Versuch und Berechnung, Ergebnis einer Zusammenarbeit zwischen der Deutschen Airbus und dem Institut für Strukturmechanik der DLR, DLR Report IB131-93/02, Braunschweig, 1993.

[11] Rolfes R., Noack J., Taeschner M., High performance 3D-Analysis of thermo-mechanically loaded composite structures, Comput. Struct. 46 (1999) 367–379.

[12] Rolfes R., Tacke S., Zimmermann R., Development and experimental verification of FE-model for stringer-stiffened fibre composite panels under combined thermal and mechanical loading conditions, in: Proceedings European Conference on Spacecraft Structures, Materials, and Mechanical Testing, November 4–6, 1998, Braunschweig, ESA SP-428, 1999, pp. 109–115.

[13] Rolfes R., Petersen D., Block J., Goetting H.-C., Hammerschmidt U., Experimental determination of the convection coefficient at the surface of a composite aircraft wing, DLR Report IB131-2000/40, Braunschweig, 2000.

[14] Stauffer W.A., James A.M., Development of advanced composite structures for Lockheed aircraft, 23rd National SAMPE Symposium/Exhibition, Anaheim, CA, 1978.

[15] Sun L.X., Hsu T.R., Thermal buckling of laminated composite plates with transverse shear deformation, Comput. Struct. 36 (1990) 883–889.

[16] Surana K.S., Orth N.J., Completely hierarchical axisymmetric shell element based on p-version for heat conduction in laminated composites, Comput. Struct. 38 (1991) 429–448.